Formation of nanowires and their interaction with atomic steps during growth of Bi on Ni(111)

Tjeerd R. J. Bollmann, Raoul van Gastel, Harold J. W. Zandvliet, and Bene Poelsema
Physics of Interfaces and Nanomaterials, MESA$^+$ Institute for Nanotechnology, University of Twente, P.O. Box 217, NL-7500AE Enschede, The Netherlands
(Received 24 June 2011; published 17 October 2011)

Using low-energy electron microscopy (LEEM) and selective area low-energy electron diffraction, we have characterized both the (7×7) wetting layer and the $BiNi_9$ $\begin{bmatrix} 2 & 0 \\ -2 & 5 \end{bmatrix}$ nanowires that form during the growth of Bi on Ni(111). The 60 ± 20 nm wide nanowires have lengths up to 10 μm and a height of 4–6 atomic layers. After the formation of the wetting layer and nanowires, quantum size effect driven growth ensues, accompanied by the gradual disappearance of the nanowires and resulting meandering of the substrate steps. The displacements of substrate steps, directly imaged with LEEM, can be traced back to dealloying.

DOI: 10.1103/PhysRevB.84.155428 PACS number(s): 61.46.Km, 73.61.At, 68.35.Gy, 68.37.Nq

I. INTRODUCTION

The self-assembly of nanostructures (the growth of nanowires) is an important topic to understand in materials science.[1,2] It is generally assumed that nanowires grow due to the competition between strain and step free energies, favoring one-dimensional structures above a certain size.[3,4] The growth of Ag wires on Si(001) is, e.g., explained by the 6% misfit strain between wire and substrate.[5] The downsizing of physical structures to small length scales can result in metal films and wires that show even more complex and different physical properties than those found for the bulk materials. For example, both strain-stabilized and electronically stabilized structures have been widely reported on in the literature.[6] A typical example of the former is the formation of a striped phase of Pb on Cu(111) as a result of a competition between the tensile and compressive strain of a PbCu surface alloy and a Pb overlayer phase.[7,8]

The formation of self-assembled nanostructures through a stabilizing interaction can be further complicated by surface alloying. Group V elements are particularly prone to this as they are known to exhibit allotropic transformations, as well as alloying on other metal substrates. Bismuth, a prototype group V element known for its allotropism, forms strained metastable thin films that exhibit phase transformations above a critical film thickness.[9,10] For Bi on Ni, the bulk alloy phase diagram reports the stoichiometric alloys BiNi and Bi_3Ni that are thermodynamically stable.[11–13] Therefore, alloying induced strain may be expected to play an important role in the growth of Bi on Ni(111). From several studies, an initial $(\sqrt{3} \times \sqrt{3})$-$R30^\circ$ surface alloy was reported.[14–17] For higher coverages, (7×7) and $(\sqrt{7/4} \times \sqrt{7/4})$-$R19^\circ$ overlayer structures were found.[14] The growth of one-dimensional nanostructures of Bi on Ni(111) has, however, not been reported in literature so far. We have previously shown Bi on Ni(111) to exhibit quantum size effect (QSE) driven growth and allotropism.[18]

In this paper, we present a study using *in situ* low-energy electron microscopy (LEEM) and selective area low-energy electron diffraction (μLEED) to probe the properties and ordering of different Bi and Bi_xNi_y film and nanowire structures. Our observations show the alloying and partial dealloying of a $(\sqrt{3} \times \sqrt{3})$-$R30^\circ$ phase, eventually leading to a (7×7) wetting layer and stable $\begin{bmatrix} 2 & 0 \\ -2 & 5 \end{bmatrix}$ $BiNi_9$ nanowires, as well as nanowires with a proposed $\begin{bmatrix} 2 & 0 \\ -3 & 4 \end{bmatrix}$ structure. The nanowires are 60 ± 20 nm wide, several microns in length, and a few atomic layers in height. Dealloying of the wetting layer as well as the gradual disappearance of the nanowires triggered by the formation of QSE stabilized structures as a result of continued deposition results in meandering of the substrate steps. These step displacements can be directly imaged with LEEM.

II. EXPERIMENT

The experiments were performed in an Elmitec LEEM III instrument. A Ni(111) single crystal was cleaned by cycles of 1-keV Ar^+ bombardment at room temperature, followed by flash annealing to a temperature of 1150 K. The cleanliness of the sample was monitored by Auger electron spectroscopy (AES) and LEEM. LEEM images revealed terraces with a width of $\sim$1 μm. All sample temperatures are subject to a measurement uncertainty of 5% and were calibrated using the uphill motion of steps over time at a temperature where sublimation is observed, as described in Ref. 19. Bismuth was deposited from a Knudsen cell.

III. RESULTS

To determine the properties of Bi on Ni(111), we performed μLEED, illuminating a circular area of 1.4 μm in diameter during deposition at 474 K. Initially, the number of secondary electrons increases when the deposition of Bi is started, indicative of the formation of an adatom gas. Subsequently, the number of secondary electrons decreases and a $(\sqrt{3} \times \sqrt{3})$-$R30^\circ$ surface alloy appears, in agreement with literature.[14] It also agrees with observations for the intimately related Pb/Ni(111) system.[15–17] Its maximum peak intensity was used to perform an *in situ* calibration of the coverage $\theta_{Bi/Ni} = 0.33$ ML, where $\theta_{Bi/Ni} = 1$ ML corresponds to 1 Bi atom per Ni surface atom. Dealloying then leads to the creation of a wetting layer. Peaks associated with an incommensurate Bi-rich overlayer appear in the μLEED pattern at a coverage of 0.45 ML. These Bi peaks shift outward with increasing coverage, indicating a continuous in-plane compression of the lattice constant. Eventually, a commensurate Bi-rich film forms with a stable (7×7) surface structure at a coverage

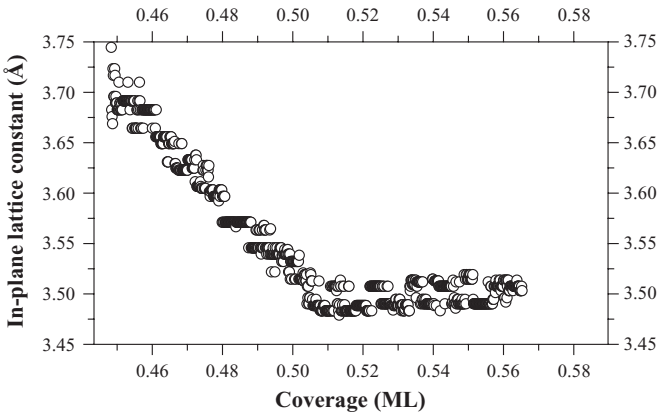

FIG. 1. The in-plane lattice constant, as derived from the position of the Bi(1,0) peak as a function of coverage at 35.0 eV during Bi deposition at 474 K. The in-plane lattice constant of 3.50 Å corresponds to the completed (7 × 7) wetting layer with a coverage of 0.510 ML.

of 0.510 ML (see Fig. 1). The commensurate (7 × 7) surface structure forms when the in-plane lattice constant stabilizes at 3.50 Å and provides another opportunity for an exact *in situ* calibration of the coverage. The measured deposition rate of 1×10^{-4} Bi atoms per unit cell (uc) per second (Bi/uc/s), or 1.86×10^{11} cm^{-2} s^{-1}, is identical to that obtained from the maximum peak intensity for the $(\sqrt{3} \times \sqrt{3})$-$R30^\circ$ surface alloy.

Assuming that at $\theta_{\mathrm{Bi/Ni}} = 0.45$ ML, dealloying of the $(\sqrt{3} \times \sqrt{3})$-$R30^\circ$ phase is complete and only Bi is populating the outermost layer, continued deposition should lead to an in-plane lattice constant compression caused by a linear increase in atomic density. One would then expect the in-plane lattice constant to be $\propto /\sqrt{ct}$, where c is the deposition rate from the vapor phase and t time. In Fig. 1, the lattice constant versus coverage is plotted, which surprisingly shows an almost linear decay. The continuous dealloying of the $(\sqrt{3} \times \sqrt{3})$-$R30^\circ$ surface alloy causes the effective deposition rate to increase linearly with time up to the coverage corresponding to the commensurate (7 × 7) surface structure: $c(t) \propto t$. Whether or not the surface alloy is completely depleted can not be deduced from this. μLEED measurements do not show ordered surface alloys for coverages $\theta_{\mathrm{Bi/Ni}} > 0.51$ ML. The Bi (7 × 7) wetting layer structure, known from literature,[14] is one atomic layer in height and covers 49 Ni unit cells, which are filled by 25 Bi atoms (see also further below).

After completion of the wetting layer, Bi nanowires appear, as can been seen in Fig. 2(a). The nanowires grow in two sets of threefold symmetric directions making an angle of 22°, shown in Fig. 2(b). The growth rate of all nanowires is similar, and becomes smaller over time. The nanowires cross underlying Ni(111) steps without an appreciable reduction in growth rate. Nanowires with a length up to about 10 μm have been observed. A simple line profile perpendicular to the nanowire gives a width of approximately 60 ± 20 nm, resulting in aspect ratios of the order of 100.

For structural characterization of the nanowire, μLEED was used with a 1.4-μm aperture. Since the width of the nanowire is orders of magnitude smaller than the diameter

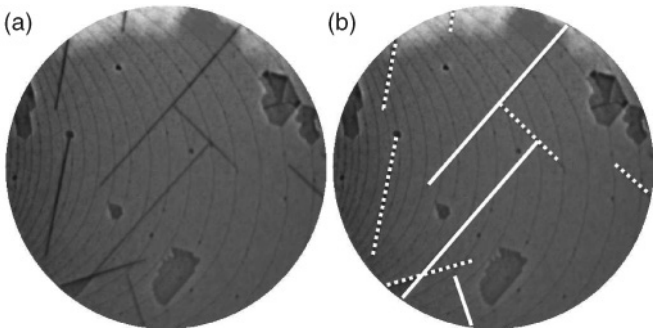

FIG. 2. (a) LEEM image with nanowires and (b) the same with full and dashed lines drawn according to the two times threefold symmetry. Field of View (FoV) = 10 μm, electron energy 2.0 eV, $T = 474$ K, $\theta_{\mathrm{Bi/Ni}} = 0.57$ ML.

of the aperture, the diffraction pattern is a superposition of two surface structures. Figure 3(a) shows a cumulative μLEED pattern of the (7 × 7) wetting layer with a nanowire present. By summing the intensities over an energy range of 3.0 to 20.0 eV, all spots forming the superstructure become visible. Figure 3(b) shows a schematic diffraction pattern with red (black) spots corresponding to the (7 × 7) wetting layer. Moving the aperture over a nanowire surrounded by wetting layer, we can identify the additional diffraction spots created by the nanowires, corresponding to the yellow (white) spots in Fig. 3(b). The superstructure short axis is, along with the (7 × 7) wetting layer, aligned with respect to the ⟨110⟩ azimuth of the substrate. The superstructure has unit-cell sides of 0.50 and 0.108 nm, making an angle of 83°, corresponding to a $\begin{bmatrix} 2 & 0 \\ -2 & 5 \end{bmatrix}$ surface alloy as illustrated in Fig. 3(c). The unit cell contains 1 Bi atom and 9 Ni atoms in one plane and its short axis is aligned with the close-packed direction of the Ni substrate. Additional information on the structure of the nanowires is obtained from a plot of the height of the (1,0) nanowire diffraction peak in Fig. 3(a) as a function of the electron energy, as is shown in Fig. 4. The intensity curve clearly shows interference features, related to the interlayer distance. From the energies corresponding to the maxima and minima, we can derive the change of the normal component of the wave vector Δk_z for in-phase conditions (the intensity maxima) n and out-of-phase conditions (the intensity minima) $n + \frac{1}{2}$, respectively, where $n \in \mathbb{N}_0$. The values for k are obtained by $k_{(\mathrm{max/min})} = 2\pi\sqrt{E_{(\mathrm{max/min})}(\mathrm{eV})/150.4}$. Due to the perpendicular geometry, $\Delta k_z = 2k$. The result is plotted in Fig. 5 and shows an ideal linear relationship. For in-phase scattering from identical planes at a vertical distance, d is required that $n\Delta k_z = 2\pi/d$. From the slope of the straight line, we obtain a vertical periodicity d of $2\pi/9.455 = 0.663$ nm. This result is puzzling since we expected a value close to 0.203 nm, the Ni(111) interlayer spacing. This surprise actually presents an unexpected opportunity to gain further insight in the structure of the nanowires. The measured periodicity is obtained when we assume that the (2 × 1) Bi chains are along $[1\bar{1}0]$ and separated by four pure Ni chains, which are present throughout the nanowire [see also Fig. 3(c)]. In other words, in the face-centered-cubic (fcc) nanowire structure, the (2 × 1) BiNi ⟨110⟩ rows fill (113) intercalation planes separated by four Bi-free (113) layers. See Fig. 3(d)

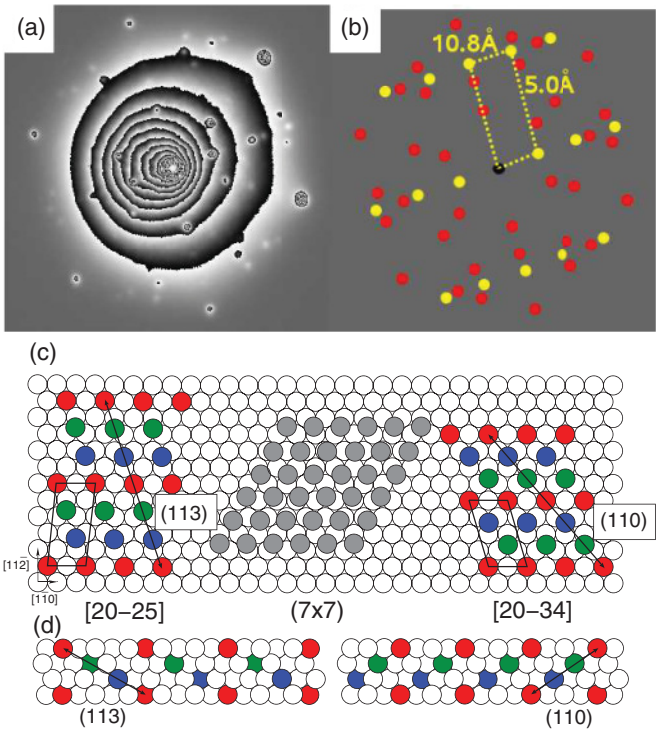

FIG. 3. (Color online) (a) Cumulative μLEED pattern for energies from 3.0 to 20.0 eV in steps of 0.1 eV for the nanowire surrounded by wetting layer. (b) Schematic diffraction pattern corresponding to Fig. 3(a), where red (dark) spots correspond to the (7 × 7) wetting layer pattern and yellow (white) spots correspond to the nanowire pattern. The superstructure of the nanowire is drawn. The short axis of the unit cell is aligned parallel to the close-packed Ni ⟨110⟩ azimuth. Panel (c) shows a top-view cartoon of the real-space unit cells for (from left to right) the $\begin{bmatrix} 2 & 0 \\ -2 & 5 \end{bmatrix}$ Bi surface alloy, the Bi (7 × 7) wetting layer, and the $\begin{bmatrix} 2 & 0 \\ -3 & 4 \end{bmatrix}$ Bi surface alloy. For the surface alloy structures, the red Bi atoms are within the top layer of the substrate plane, which at the same time is the first layer of the nanowire. The blue Bi atoms are in the second nanowire layer. The green Bi atoms are in the third layer. The fourth layer Bi atoms are then in the red positions again. In other words, the Bi nanowire is viewed as a Bi-containing Ni fcc film with fcc structure. The Ni atoms in the higher layers are not shown for display purpose. Panel (d) shows the cross-sectional view of the Bi surface alloys for a four-layer-high structure. For the two Bi surface alloys, the (113)- and the (110)-intercalation planes are indicated. The Bi-rich directions are the $[1\bar{1}0]$ direction and the $[12\bar{1}]$ and $[1\bar{1}2]$ directions that define the (113) and (110) planes, respectively.

for a cross-sectional view illustration. Note that intercalated structures have been found for other BiNi alloys.[11,20] As a consequence, the (111)-interlayer spacing is found to be 0.22 nm, i.e., marginally larger than the Ni value. In order to observe the measured interference effects, the film has to be at least four layers thick. An even stronger interference would result from a thicker film with, for instance, a height of six layers. The thickness of the nanowires must therefore be at least 0.66 nm. This is further discussed below. Note that the width of the (1,0) nanowire diffraction peaks is constant within the error margins, making interference due to atomic steps improbable.[21] This provides support for the assumption that the interference effects responsible for the particular behavior

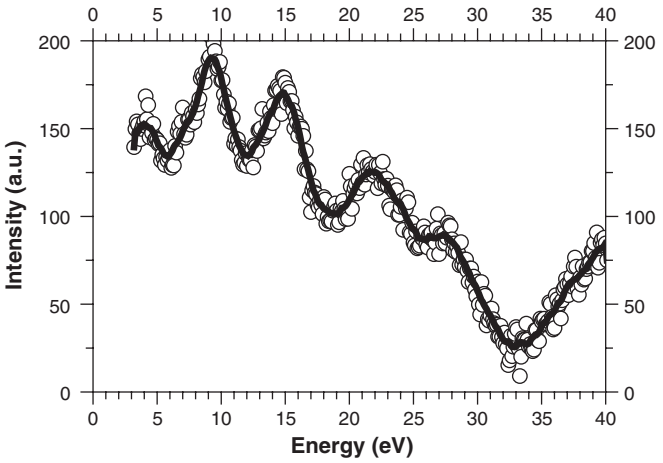

FIG. 4. I/V-μLEED data obtained from the (1,0) peak of the structure shown in Fig. 3(a). The maxima and minima are used to calculate Δk_z components in Fig. 5. A linear background profile has been subtracted. The solid line serves as a guide to the eye.

of the peak height in Fig. 4 are due to interference inside the crystal.

Shortly after nucleation of the $BiNi_9$ nanowires, different, coexisting domains with different heights and crystal structures appear, which are electronically stabilized through the accommodation of their specific Fermi wavelength. [Thee films show (3 × 3) and matrix structure ($m_{11} = 3$, $m_{12} = -1$, $m_{21} = 1$, $m_{22} = 2$) ordering with thicknesses of, respectively, three and five atomic layers.] The details of the electronic growth of these film structures are discussed elsewhere.[18] Figure 6 shows these QSE stabilized islands, labeled with their height of three and five atomic layers. The height is measured with respect to the bare Ni(111) substrate. Two parallel nanowires are highlighted by the text nanowire. As the coverage is increased, we observe the QSE stabilized island

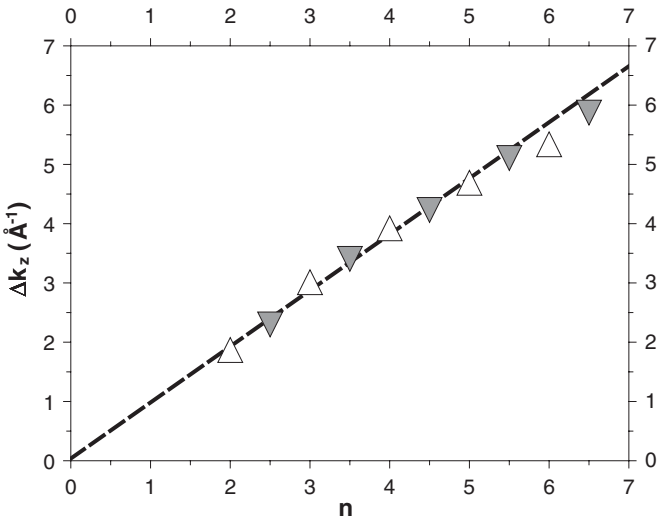

FIG. 5. Calculated Δk_z values found for in-phase n (up triangles) and out-of-phase $n + \frac{1}{2}$ (down triangles) conditions from the maxima and minima in the I/V-μLEED data shown in Fig. 4. The dashed line has a slope of 0.9455 Å^{-1}, where the coefficient of determination equals 0.991.

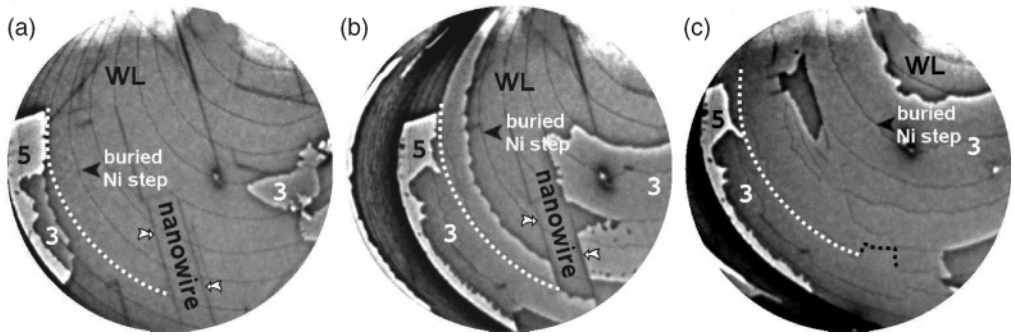

FIG. 6. (a)–(c) LEEM images showing nanowires [marked by white arrows in (a) and (b)] acting as limitations for the expansion of the electronic driven growth of the domains. Dealloying of the nanowires and the wetting layer results in meandering steps. QSE driven islands are labeled with their respective height, WL denotes the (7×7) wetting layer. The initial Ni(111) substrate steps appear as curved dark lines; examples of these buried Ni steps are indicated by black arrows. An example of a meandering substrate step is indicated by the white dashed line, where the movement of the step position near a disappearing nanowire is shown by the black dashed line in (c). FoV =10 μm, electron energy 2.0 eV, $T = 474$ K, (a) $\theta_{\mathrm{Bi/Ni}} = 0.65$ ML, (b) $\theta_{\mathrm{Bi/Ni}} = 1.00$ ML, (c) $\theta_{\mathrm{Bi/Ni}} = 1.35$ ML.

of height three, on the left in Fig. 6, to cross steps of the substrate. We observe a slight roughening of the steps with increasing coverage upon examining the position of the step marked by the white dashed line [see Figs. 6(b) and 6(c)]. We also see a significant displacement in the downward direction, from bottom left to top right. From this observation, as well as our coverage calibration, we conclude that the (7×7) wetting layer is not exclusively composed of Bi atoms, but in fact comprises the underlying substrate top layer as well. The (7×7) wetting layer has to contain a small amount of Ni, with the substrate top layer holding an equally small amount of Bi. The growth of QSE stabilized structures then leads to reordering of the wetting layer, fully dealloying the Bi and Ni in the process. The Ni then attaches to steps, causing them to meander slightly.

Figure 6(b) shows the blocking of the growth front of the QSE stabilized structure by a nanowire. As soon as the nanowire is surrounded by the three-layer-high structure, the nanowire gradually disappears into the QSE stabilized structure. Since the nanowires consist of 90% Ni atoms, their gradual disappearance also leads to meandering of steps in the downward direction, as shown in Fig. 6(c) by the black dashed line. By measuring the increase in terrace area due to the step advancement as a result of the dealloying of the nanowires with a 10% Bi content, the height of the nanowires is estimated to be 3.9 ± 0.5 layers, in agreement with the previous analysis from the I/V-μLEED measurement in Fig. 4.

IV. DISCUSSION

From the observations in the diffraction pattern in Fig. 3(a), in combination with the analysis (see Fig. 5) of the interference data in Fig. 4, we come to the following two hard conclusions: the periodicity perpendicular to the surface is tripled with respect to the Ni(111) interlayer distance and the periodicity along the [110] azimuth is doubled with respect to the Ni(111) surface. This leads to two principal choices for the alloy composition, either Bi_9Ni or $BiNi_9$. Since the atomic numbers for Bi and Ni differ strongly, the scattering factor for Bi is thus much larger than for Ni. Consequently, the Bi-rich variant would be extremely hard to reconcile with the distinct three-layer periodicity perpendicular to the surface, which then would incline more toward the single-layer periodicity. As we described just above, the $BiNi_9$ structure also fits nicely to the meandering step edges at the Ni/Bi interface upon annihilation of the nanowires [see e.g. Fig. 6(c)]. Combination of these facts provides a strong base for the $BiNi_9$ assignment.

From the cumulative μLEED pattern in Fig. 3(a), the surface structure of one of the threefold-symmetric nanowire types is found to be $\left[\begin{smallmatrix} 2 & 0 \\ -2 & 5 \end{smallmatrix}\right]$. Since the distance between embedded Bi atoms is smallest along the $[12\bar{1}]$ direction, being $\sqrt{3} \times a_{\mathrm{nn}}$, with a_{nn} the Ni nearest-neighbor distance, we expect the nanowires to grow along the $[\bar{3}21]$ azimuth. This actually offers an attractive explanation for the observation of approximately perpendicular nanowires (see Fig. 2), which are symmetry forbidden on a fcc(111) surface. Note that microfacets of steps seen along the $[11\bar{2}]$ azimuth have a (100) orientation, while those seen along the $[\bar{1}\bar{1}2]$ azimuth have a (111) orientation [see also Fig. 3(c)]. With an evaluation scheme similar to the one leading to (113) Bi-rich planes intercalated with Bi-poor planes in a ratio of 1 to 5, we arrive at Bi-rich lines along $[1\bar{1}0]$ and $[1\bar{1}2]$ directions, which set up (110) planes as shown in Figs. 3(c) and 3(d) (right). The corresponding unit cell is written as $\left[\begin{smallmatrix} 2 & 0 \\ -3 & 4 \end{smallmatrix}\right]$. The Bi content in this structure is 12.5%. From the smallest Bi distance of $\sqrt{3} \times a_{\mathrm{nn}}$, the corresponding propagation direction of these nanowires is to be expected along the $[\bar{3}12]$ azimuth. As a consequence, both sets of nanowires have angles of 22° or 82°, i.e., consistent with the angles measured in Fig. 2. Unfortunately, we have not been able to collect sufficiently reliable data for the latter set of nanowires and the (110) Bi-rich intercalated plane in a 1 to 4 ratio remains a speculation here. Both structures, however, do possess the essential property that is necessary for the formation of nanowires. The placement of the Bi atoms in the (113) and (110) crystal planes of both types of nanowires induces an anisotropy in the alloying induced strain. This is a key requirement for the structure to form nanowires.[3,4]

Both the height and structure of the $BiNi_9$ nanowires have been characterized by (I/V-)μLEED. The periodicity perpendicular to the surface corresponds to three (111) Ni

layers in a fcc stacking configuration, containing 10% Bi. In principle, the interference could be the result of steps in the vacuum-nanowire interface too. The fact that the straight line in Fig. 5 intersects the origin, thereby indicating a negligible inner potential difference, seems to suggest that. However, the discussed interference effect should give rise to peak broadening under destructive interference conditions (see, e.g., Ref. 21). Such effects are not supported by the experimental data, which could be due to the transfer width of the instrument in combination with the length scale of the atomic steps. However, since more explanations for the intersection of the origin in Fig. 5 may apply, including, e.g., relaxation within the nanowire, we are inclined to think in terms of a well-defined and constant height of the nanowires across their width profile.

V. SUMMARY

Using LEEM and μLEED, we have characterized both the (7×7) wetting layer and $BiNi_9$ nanowires. The nanowires show lengths up to about 10 μm. Making use of I/V-μLEED data, we found the height of the nanowires to be 4–6 atomic layers with respect to the substrate. The nanowires assume a $\begin{bmatrix} 2 & 0 \\ -2 & 5 \end{bmatrix}$ superstructure, containing 90% Ni. With the limitations set by the small width of the nanowires in mind, we conclude that the nanowires have a fcc stacking with each fifth (113) intercalated plane containing 50% Bi. Due to the incomplete dealloying of the $(\sqrt{3} \times \sqrt{3})$-$R30^\circ$ surface alloy at coverages $\theta_{\mathrm{Bi/Ni}} > 0.33$ ML, the (7×7) wetting layer in fact comprises two layers of which the lower one, the top substrate layer, contains a small but finite Bi content. The (7×7) wetting layer may contain a minor fraction of Ni. Upon the QSE driven growth of three- and five-layer-high structures on top of the bare Ni(111) substrate, dealloying of the wetting layer and nanowires results in meandering of steps in the step-down direction, as is imaged with LEEM.

ACKNOWLEDGMENT

This work is part of the research programme of the Foundation for Fundamental Research on Matter (FOM), which is financially supported by the Netherlands Organization for Scientific Research (NWO).

[1] Y. Cui, Q. Wei, H. Park, and C. Lieber, Science **293**, 1289 (2001).
[2] S. Evoy, N. DiLello, V. Deshpande, A. Narayanan, H. Liu, M. Riegelman, B. R. Martin, B. Hailer, J.-C. Bradley, W. Weiss *et al.*, Microelectron. Eng. **75**, 31 (2004).
[3] A. Li, F. Liu, and M. G. Lagally, Phys. Rev. Lett. **85**, 1922 (2000).
[4] H. J. W. Zandvliet and R. van Gastel, Phys. Rev. Lett. **99**, 136103 (2007).
[5] J. Tersoff and R. M. Tromp, Phys. Rev. Lett. **70**, 2782 (1993).
[6] B. J. Hinch, C. Koziol, J. P. Toennies, and G. Zhang, Europhys. Lett. **10**, 341 (1989).
[7] R. Plass, N. C. Bartelt, and G. L. Kellogg, J. Phys. Condens. Matter **14**, 4227 (2002).
[8] R. van Gastel, R. Plass, N. C. Bartelt, and G. L. Kellogg, Phys. Rev. Lett. **91**, 055503 (2003).
[9] S. Yaginuma, K. Nagaoka, T. Nagao, G. Bihlmayer, Y. M. Koroteev, E. V. Chulkov, and T. Nakayama, J. Phys. Soc. Jpn. **77**, 014701 (2008).
[10] T. Nagao, J. T. Sadowski, M. Saito, S. Yaginuma, Y. Fujikawa, T. Kogure, T. Ohno, Y. Hasegawa, S. Hasegawa, and T. Sakurai, Phys. Rev. Lett. **93**, 105501 (2004).
[11] P. Nash, J. Phase Equilib. **6**, 345 (1985).
[12] P. Feschotte and J.-M. Rosset, J. Less-Common Met. **143**, 31 (1988).
[13] G. P. Vassilev, X. J. Liu, and K. Ishida, J. Phase Equilib. Diffus. **26**, 161 (2005).
[14] K. Gürtler and K. Jacobi, Surf. Sci. **152–153**, 272 (1985).
[15] K. Umezawa, A. Takahashi, T. Yumura, S. Nakanishi, and W. M. Gibson, Surf. Sci. **365**, 118 (1996).
[16] K. Umezawa, S. Nakanishi, T. Yumura, W. M. Gibson, M. Watanabe, Y. Kido, S. Yamamoto, Y. Aoki, and H. Naramoto, Phys. Rev. B **56**, 10585 (1997).
[17] D. Brown, P. D. Quinn, D. P. Woodruff, P. Bailey, and T. C. Q. Noakes, Phys. Rev. B **61**, 7706 (2000).
[18] T. R. J. Bollmann, R. van Gastel, H. J. W. Zandvliet, and B. Poelsema, Phys. Rev. Lett. **107**, 176102 (2011).
[19] M. Ondrejcek, M. Rajappan, W. Swiech, and C. P. Flynn, Phys. Rev. B **73**, 035418 (2006).
[20] S.-K. Seo, M. G. Cho, and H. M. Lee, J. Electron. Mater. **36**, 1536 (2007).
[21] L. K. Verheij, B. Poelsema, and G. Comsa, Surf. Sci. **162**, 858 (1985).